FAWCETT, J. K. & TROTTER, J. (1965). *Proc. R. Soc. London Ser. A*, **289**, 366–376.
FERRARIS, G., JONES, D. W. & YERKESS, J. (1973). *Z. Kristallogr.* **138**, 113–128.
HABERDITZL, W. (1976). *Theory and Applications of Molecular Diamagnetism*, pp. 59–233. New York: Wiley–Interscience.
HAZELL, A. C., LARSEN, F. K. & LEHMANN, M. S. (1972). *Acta Cryst.* B**28**, 2977–2984.
JONES, D. W. & YERKESS, J. (1971). *J. Cryst. Mol. Struct.* **1**, 17–23.
KAY, M. I., OKAYA, Y. & COX, D. E. (1971). *Acta Cryst.* B**27**, 26–33.
KRISHNAN, K. S. & BANERJEE, S. (1935). *Philos. Trans. R. Soc. London Ser. A*, **234**, 265–298.
LANDOLT-BÖRNSTEIN (1967). Band II, Teil 10, *Magnetische Eigenschaften* II. Berlin: Springer.
LASHEEN, M. A. (1968). *Acta Cryst.* A**24**, 289–295.
LE FÈVRE, R. J. W. & MURTHY, D. S. N. (1966). *Aust. J. Chem.* **19**, 179–186.
LE FÈVRE, R. J. W. & MURTHY, D. S. N. (1969). *Aust. J. Chem.* **22**, 1415–1419.
LONSDALE, K. & KRISHNAN, K. S. (1936). *Proc. R. Soc. London Ser. A*, **156**, 597–613.
LUMBROSO-BADER, N. (1956). *Ann. Chim.* **13**(1), 657–744.
MASON, R. (1964). *Acta Cryst.* **17**, 547–555.
PULLMAN, B. & PULLMAN, A. (1952). *Les Théories Electroniques de la Chimie Organique*. Paris: Masson et Cie.
POQUET, E. (1963). Thèse n° 123. Bordeaux.
ROBERTSON, J. M. & WHITE, J. G. (1956). *J. Chem. Soc.* 925–931.
ROGERS, M. T. (1947). *J. Am. Chem. Soc.* **69**, 1506–1508.
VAN DEN BOSSCHE, G. & SOBRY, R. (1974). *Acta Cryst.* A**30**, 616–625.
VAN DEN BOSSCHE, G. & SOBRY, R. (1981). En préparation.

Acta Cryst. (1981). A**37**, 219–226

Investigation and Interpretation of Diffuse X-ray Scattering in Li_3N

BY R. SOMMER, HEINZ SCHULZ AND W. KRESS

Max-Planck-Institut für Festkörperforschung, Heisenbergstrasse 1, 7000 *Stuttgart* 80, *Federal Republic of Germany*

(*Received* 26 *June* 1980; *accepted* 1 *October* 1980)

Abstract

Diffuse X-ray scattering in Li_3N has been investigated in the range 293 to 880 K with monochromatic Mo $K\alpha$ radiation. Crystal and film were fixed during the exposure. Diffuse intensity in the form of rods and discs was found. It increased with increasing temperature but without change of its features. The diffuse intensity distribution was calculated for various temperatures on the basis of an anisotropic shell model. Good agreement with the experimental results was achieved. The anharmonic effects detected in the difference electron density were studied taking into account split positions for the Li ions. This simulation leads to only minor changes in the calculated intensity distribution which indicates that the diffuse intensity of Li_3N is mainly caused by harmonic lattice vibrations.

Introduction

Li_3N is of interest for both fundamental and technical reasons. Being a fast ionic conductor with Li^+ ions as conducting species it offers technical application in high-energy-density batteries (von Alpen, 1979). Fundamental interest is concerned with the fact that Li_3N is a superionic conductor which shows nearly complete ordering (Schulz & Thiemann, 1979). This is in contrast with other fast ionic conductors, such as AgI and β-alumina which reveal a large degree of occupational disorder (Huggins & Rabenau, 1978).

The ionic conductivity of Li_3N has been investigated by Boukamp & Huggins (1976) for polycrystalline samples and by von Alpen, Rabenau & Talat (1977) and von Alpen, Bell & Gladden (1979) for single crystals. von Alpen, Rabenau & Talat (1977) found a strong anisotropy for the conductivity with an activation energy of 0·29 eV perpendicular to and 0·49 eV parallel to **c**. Studies of Li_3N ceramics for technical applications have been carried out (von Alpen, Bell & Gladden, 1979).

Zintl & Brauer (1935) proposed a hexagonal structure model for Li_3N in space group $P6/mmm$. In this model the N ions are surrounded by eight Li ions in the form of a hexagonal bipyramid (Fig. 1). This structure can also be considered as a layer structure with alternating Li_2N layers and Li layers perpendicular to **c**. Within a Li_2N layer each N ion is surrounded by six Li ions, labelled Li(2). These layers are connected by one N–Li–N bond per elementary

0567-7394/81/020219-08$01.00

cell, which coincides with **c**. The Li ions in the pure Li layers are labelled Li(1). A reinvestigation of the crystal structure by Rabenau & Schulz (1976) confirmed the structure of Zintl & Brauer (1935).

Structure investigations by Schulz & Schwarz (1978) and Schwarz & Schulz (1978) revealed the existence of N^{3-} ions in Li_3N. Dielectric measurements at low temperatures showed the existence of a local ionic motion in a shallow potential (Wahl & Holland, 1978).

Schulz & Thiemann (1979) and subsequently Schulz & Zucker (1979) investigated the defect structure up to about 900 K. They found that the Li(1) positions were completely occupied at all temperatures. However, 1% of the Li(2) positions are vacant at room temperature. With increasing temperature the number of vacancies in the Li_2N layer increases reaching about 13% at 900 K.

Schulz & Thiemann (1979) and Schulz & Zucker (1979) showed by difference maps that the diffusion of the Li^+ ions takes place on diffusion paths surrounding the N^{3-} ions within the Li_2N layers. Parallel to **c** the Li^+ ions jump from occupied Li(2) positions to unoccupied Li(2) positions in neighbouring Li_2N layers.

NMR measurements by Messer, Birli & Differt (1980) and by Brinkmann, Freudenreich & Ross (1978) confirmed the general model of the ionic diffusion process. In addition they found jumps along a path connecting the positions Li(2)–Li(1)–Li(2). The NMR measurements of Differt & Messer (1980) supported the idea of ionic bonding in Li_3N. Recent results on Li_3N are reviewed by Rabenau (1978).

In this paper we report on the investigation of diffuse X-ray scattering in Li_3N as well as on the results of calculations of diffuse intensity distributions based on an anisotropic shell model.

The starting point for this work was the observation of unusually strong diffuse X-ray scattering from Li_3N. It is a fast ionic conductor and lattice-dynamical calculations have revealed low-frequency phonon modes. It was our aim to elucidate the relations between these observations.

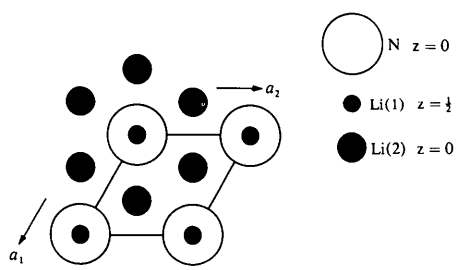

Fig. 1. Projection of the Li_3N structure along **c**.

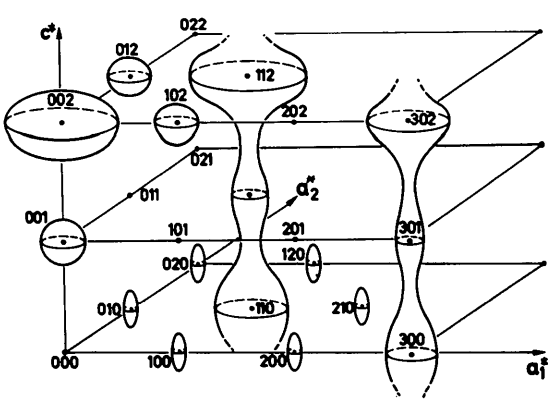

Fig. 2. Schematic drawing of the diffuse intensity in an asymmetric unit of the reciprocal space of Li_3N.

Experimental investigation

I. *Technique*

The crystals used were grown by the Czochralski method (Schönherr, Müller & Winkler, 1978). Pieces with faces $(0{\cdot}7\ \text{mm})^2$ and several mm in length were prepared. It was thereby possible to use a large diffracting volume to obtain more diffracted intensity. The crystals were enclosed in tubes of Lindemann glass to prevent reaction with the atmosphere. The tubes were mounted on a precession camera with **c** parallel to the dial axis.

An oven allowed the heating of the crystals up to more than 900 K with a precision of ± 2–3 K. Diffraction photographs of the diffuse intensity were taken in the range 290 to 880 K. The crystals were irradiated by monochromatic Mo $K\alpha$ radiation. The absorption could be neglected. The exposure time was 24 h. During that time crystal and film were fixed. This means that the diffuse intensity distribution on a segment of the Ewald sphere in reciprocal space was registered on the film according to the specific orientation of the crystal. Between subsequent exposures the crystal was turned by 2° about the dial axis. In this way we obtained a series of diffraction photographs of the diffuse intensity distribution in a volume of reciprocal space which is approximately given by $-3 < h < 3$, $-3 < k < 3$, $-3 < l < 3$. The diffuse intensity increased with increasing temperature without changing its structure. The most important features are (Fig. 2):

– diffuse rods joining the Bragg peaks $11l$ and $30l$;

– diffuse discs perpendicular to $\mathbf{c}^*$ in the layer $l = 2$;

– no diffuse intensities around the reflections 101 and 201.

Inspection shows that the strong diffuse intensities decrease with increasing distance from the Bragg peaks. Furthermore, a relation is found between the intensities of the Bragg peaks and the diffuse intensities around them.

This explains:

– the absence of diffuse intensities around 101 and 201, as these reflexions have very weak intensites;

– the high diffuse intensities around the reflexions $11l$ and $30l$ because these belong to the reflexions with the strongest intensities.

II. *Intensity calculations*

(*a*) *Lattice-dynamical model.* The calculation of the intensities for thermal X-ray scattering requires the knowledge of phonon frequencies $\omega(\mathbf{q}_j)$ and eigenvectors $\mathbf{e}(k,\mathbf{q}_j)$ in the whole Brillouin zone. To calculate these frequencies and eigenvectors we used a model which takes into account:

(i) short-range repulsive interactions between N^{3-} and $Li^+(1)$ and between N^{3-} and $Li^+(2)$ (five parameters);

(ii) long-range Coulomb interaction between all ions;

(iii) the high and anisotropic polarizability of the N^{3-} ions within the framework of an anisotropic shell model (three parameters).

The electrostatic interactions are calculated by the Ewald method. The ionic charges are assumed to be $-3e$ and $+e$ for N and Li respectively. Up to this point the model is identical to that proposed by Chandrasekhar, Bhattacharya, Migoni & Bilz (1978). Owing to elimination of a numeric error in the calculation of Chandrasekhar *et al.* (1978) and to a description of the acoustic modes which is consistent with the requirements of elastic theory, the correct results (Kress, Grimm, Press & Lefebvre, 1980) given in Fig. 3(*a*) and (*b*) are quite different from those calculated by Chandrasekhar *et al.* (1978). The results presented here are in agreement with recent results of inelastic neutron scattering measurements by Kress *et al.* (1980). In this paper a detailed discussion of the lattice-dynamical model is given. It should be noted that the lowest branch in the $[00\xi]$ direction (Fig. 3*a*) is a twofold degenerate transverse acoustic E_1 branch with polarization vectors in the basal plane. The lowest acoustic branch propagating in the $[0\xi0]$ and $[\xi\xi0]$ directions in the basal plane has polarization vectors parallel to **c**.

(*b*) *Calculation of diffuse intensity distribution.* In a first approximation the expression for the time-averaged diffuse intensity from lattice vibrations, called the dynamical structure factor, is (Willis & Pryor, 1975):

$$I(\mathbf{Q}) = \sum_j \frac{E(\mathbf{q}_j)}{N\omega^2(\mathbf{q}_j)} \left| \sum_k \frac{f_k(\mathbf{Q})}{M_k} e^{-W_k(\mathbf{Q})}\, \mathbf{Q}.\mathbf{e}(k,\mathbf{q}_j)\, e^{i\mathbf{H}.\mathbf{r}_k} \right|^2, \quad (1)$$

where **H** is a vector of the reciprocal lattice, **q** the propagation vector of the phonons, $\mathbf{Q} = \mathbf{q} + \mathbf{H}$ the momentum transfer vector, $f_k(\mathbf{Q})$ the atomic scattering factor, $e^{-W_k(\mathbf{Q})}$ the anisotropic temperature factor, $\mathbf{r}_k$ the position vector of ion k in the unit cell, j the branch index of the phonon modes, M_k the mass of the atom k, $E(\mathbf{q}_j)$ the energy of the mode $(\mathbf{q}_j)$, $\mathbf{e}(k,\mathbf{q}_j)$ the eigenvector of atom k in mode $(\mathbf{q}_j)$, and N the number of unit cells.

According to this expression diffuse intensities at the point **Q** in reciprocal space are generated by phonons with the wave vector $\mathbf{q} = \mathbf{Q} - \mathbf{H}$. Small $\omega(\mathbf{q}_j)$ values and large displacements $\mathbf{e}(k,\mathbf{q}_j)$ for a given **q** cause large intensities. Generally the acoustic modes have smaller frequencies than optical modes and therefore give the main contributions to the diffuse intensities. The general feature of decreasing diffuse intensity with increasing distance from a Bragg peak is explained by the fact that the frequency of the acoustic modes increases rapidly with increasing **q**, *cf.* Fig. 3.

The anisotropic temperature factor has been calculated in the form (Willis & Pryor, 1975)

$$e^{-W(\mathbf{Q})} = \exp\left(-\sum_{i,j=1}^{3} B_{ij} h_i h_j\right). \quad (2)$$

The B_{ij} are related to the mean-square displacements by

$$B_{ij} = 2\pi^2 u_{ij}\, \mathbf{a}_i^*\, \mathbf{a}_j^*. \quad (3)$$

The numerical values are determined by structure refinement (Schulz & Thiemann, 1979).

The diffuse intensity distribution was calculated according to (1) for various **Q** vectors and plotted for comparison with the diffraction photographs in Figs. 5 to 10. The background intensity originating from the

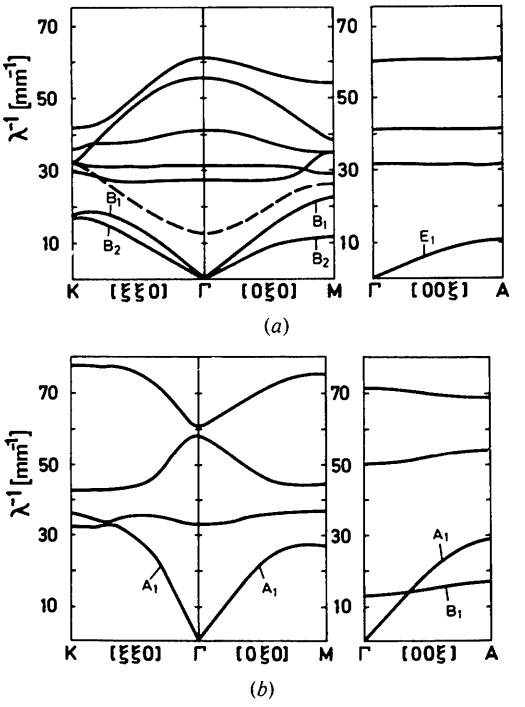

Fig. 3. Dispersion curves of Li_3N. Phonon dispersion curves taken from Kress *et al.* (1980). ξ: reduced wave-vector coordinate. (*a*) Transversal modes, (*b*) longitudinal modes.

Lindemann-glass tube which encloses the crystals is superposed on the diffuse intensity on the diffraction film. This background intensity is shown in Fig. 4. However, good agreement between experimental and theoretical results is apparent. The diffuse rods along $11l$ and $30l$ as well as the disk for $l = 2$ are reproduced by the calculation. The variation of intensity around Bragg peaks is similar to that determined experimentally.

We have performed the calculations for 293, 473 and 673 K (Figs. 5 and 11). We find an increase of the diffuse intensity with increasing temperature but no change in its features in agreement with experimental results.

It is possible to relate the main features of the diffuse intensity distribution to the dispersion curves given in Fig. 3. The rod-like structure along $11l$ and $30l$ is mainly caused by the low-frequency transverse acoustic mode E_1 in the $[00\xi]$ direction which is twofold degenerate. The disc-like structure for $l = 2$ is generated mainly by the lowest transverse acoustic B_2 mode in the $[0\xi0]$ direction.

However, for the good agreement achieved here it is necessary to take account of the contributions of all modes. This is shown in Fig. 12 where the intensity distribution is calculated by taking into account only the lowest branches. The general structure is reproduced but the agreement with the diffraction photograph is unsatisfactory (*cf.* Fig. 9*a*).

(*c*) *Modification of the theoretical model.* From the investigation of the ionic conductivity and from the experimental results of Schulz & Thiemann (1979) and Schulz & Zucker (1979) it is evident that only part of the dynamics of the Li ions in Li_3N can be described by the harmonic approximation. To simulate the effects of anharmonicity seen in the difference electron density we modified the model in the following way: three split positions for the Li(2) ions were introduced in the Li_2N layer, each one occupied by a fraction p_2. The remaining Li(2) ions were left at their regular positions.

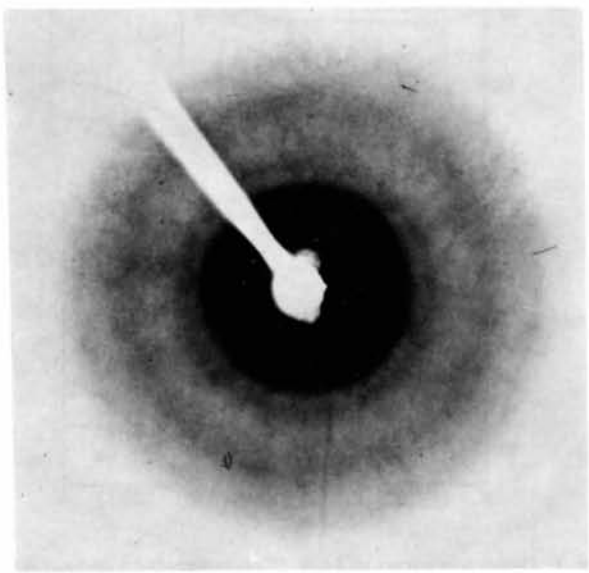

Fig. 4. Diffuse background originating from diffraction of the Lindemann-glass tube.

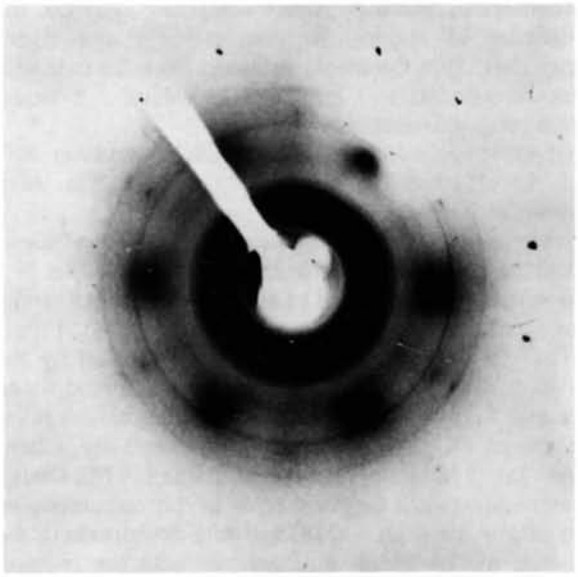

(*a*)

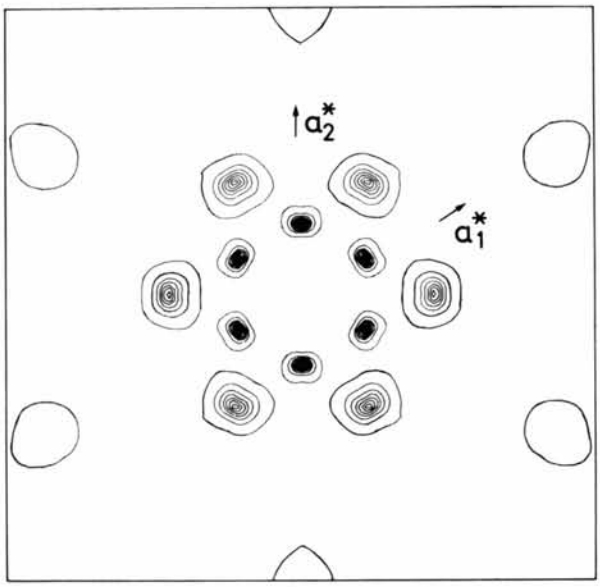

(*b*)

Fig. 5. Observed (*a*) and calculated (*b*) diffuse X-ray intensities. $T = 473$ K. The ring-like diffuse scattering around the centre of the diffraction photograph in (*a*) originates from the Lindemann-glass tube surrounding the crystal (*cf.* Fig. 4). The black spots within the areas of calculated intensities in (*b*) are regions of very high diffuse intensity in the direct neighbourhood of a Bragg reflection. Fixed film–fixed crystal technique. Film perpendicular to the X-ray beam. Monochromatic Mo $K\alpha$ raidation. Orientation of the crystal: ($\mathbf{a}_1^*$, $\mathbf{a}_2^*$) plane parallel to the film.

All ions were assumed to vibrate harmonically, independently of the position at which they were actually situated. This model is shown in Fig. 13.

It is a rather simple model. However, it offers the possibility of studying the modifications of the diffuse intensity distribution by choosing appropriate values for the occupation probability p_2 of the split positions and the distance between the split position and the regular position. They were chosen to be $p_2 = 0{\cdot}02$ and $d = 0{\cdot}1a$ (a = lattice constant) respectively. The density plot obtained with these parameters is practically identical with Fig. 9(*b*), even though the values for the parameters chosen are rather large for temperatures between 500 and 600 K. This suggests that anharmonicity has little effect on the diffuse intensity distribution.

Discussion

Ionic conduction and corresponding diffusion paths in Li_3N have been investigated by von Alpen, Rabenau &

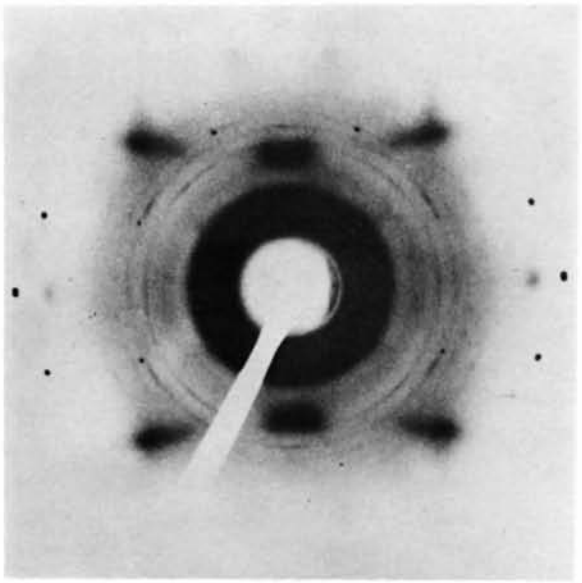

(*a*)

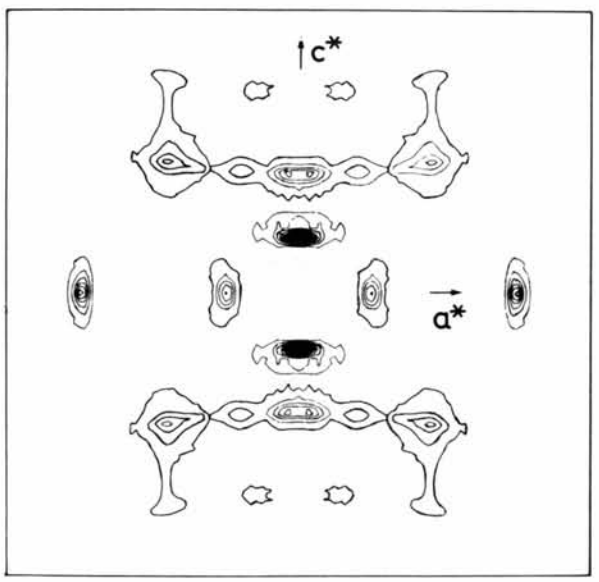

(*b*)

Fig. 6. Details as in Fig. 5; ($\mathbf{c}^*$, $\mathbf{a}_1^*$) plane parallel to the film. The zig-zag form of some of the lines in (*b*) is an artifact caused by the interpolation procedure.

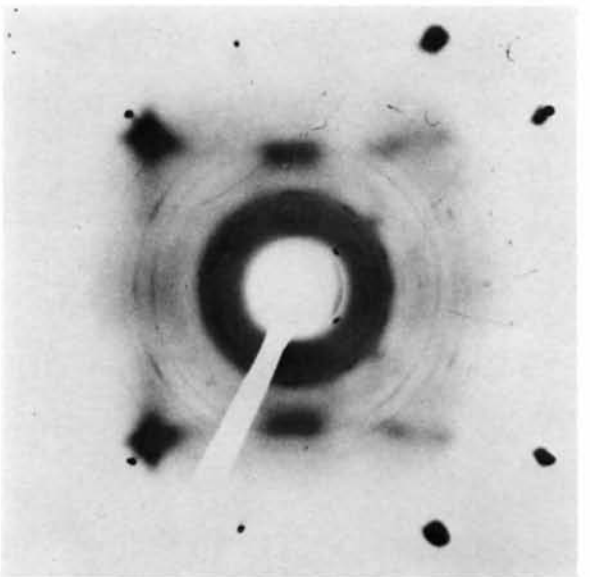

(*a*)

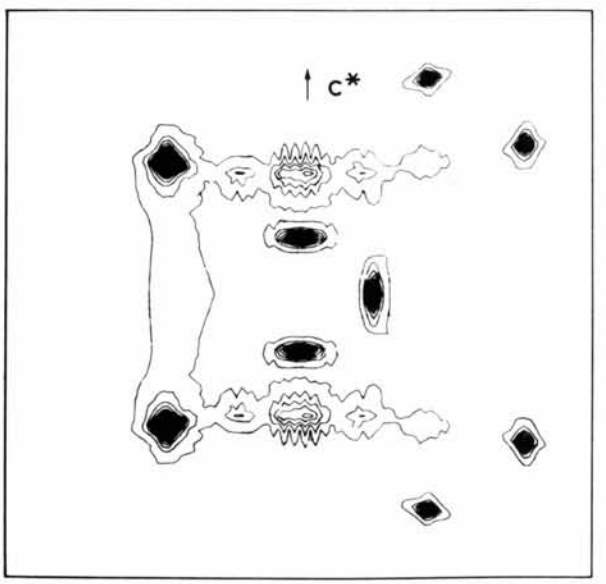

(*b*)

Fig. 7. Details as in Fig. 5; $\mathbf{c}^*$ parallel to film, $\mathbf{a}_1^*$ inclined by 6° to the film.

Talat (1977), Schulz & Thiemann (1979) and Schulz & Zucker (1979). In this paper we report on diffuse X-ray scattering. The diffuse intensities are mainly caused by harmonic lattice vibrations. The introduction of anharmonic extensions of the harmonic model had little effect on the calculated intensity distribution. But this does not rule out anharmonic parts of the crystal potential; it only means that in our case it is not possible to get detailed information about anharmonicity by diffuse X-ray scattering experiments. The reason for this is that diffuse intensity is caused by the coherent vibrations of large regions in the crystal in which all ions are taking part. In contrast to this the diffusion is the sum of a large number of individual processes which are relatively independent of each other. Furthermore, only the Li^+ ions are involved in the diffusion and not the strongly diffracting N^{3-} ions. Therefore the diffusion causes a negligible intensity compared to the intensity of the harmonic vibrations. There are, however, some indications of the diffusion process: the rod-like diffuse structure parallel to $\mathbf{c}^*$ is mainly generated by the low-lying phonons of the branch E_1.

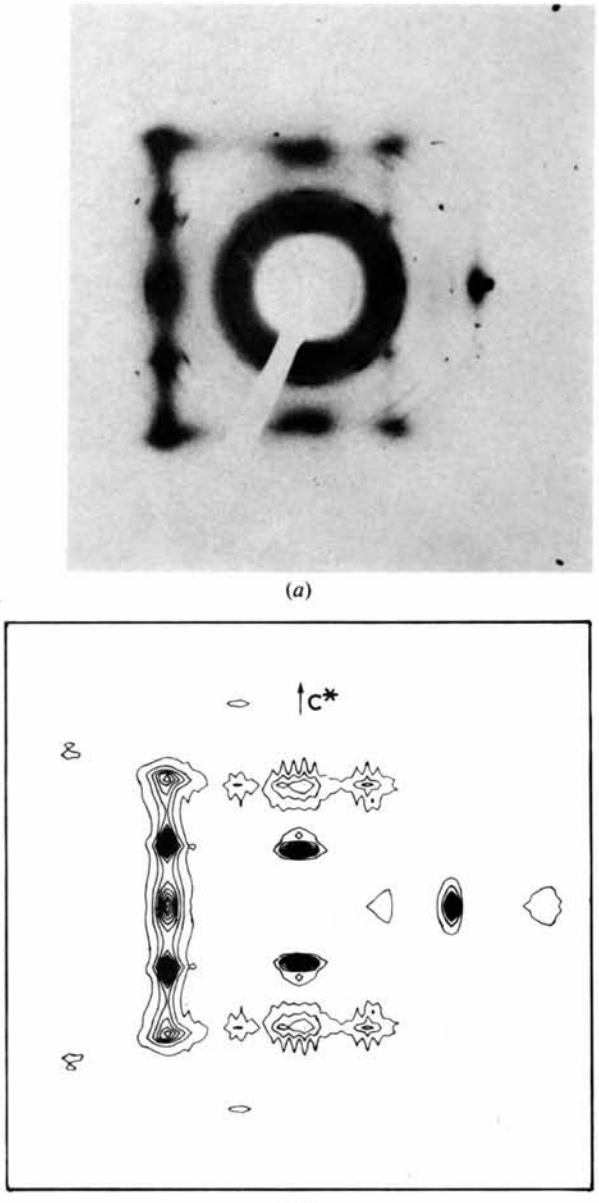

Fig. 8. Details as in Fig. 5; $\mathbf{c}^*$ parallel to film, $\mathbf{a}_1^*$ inclined by 14° to the film.

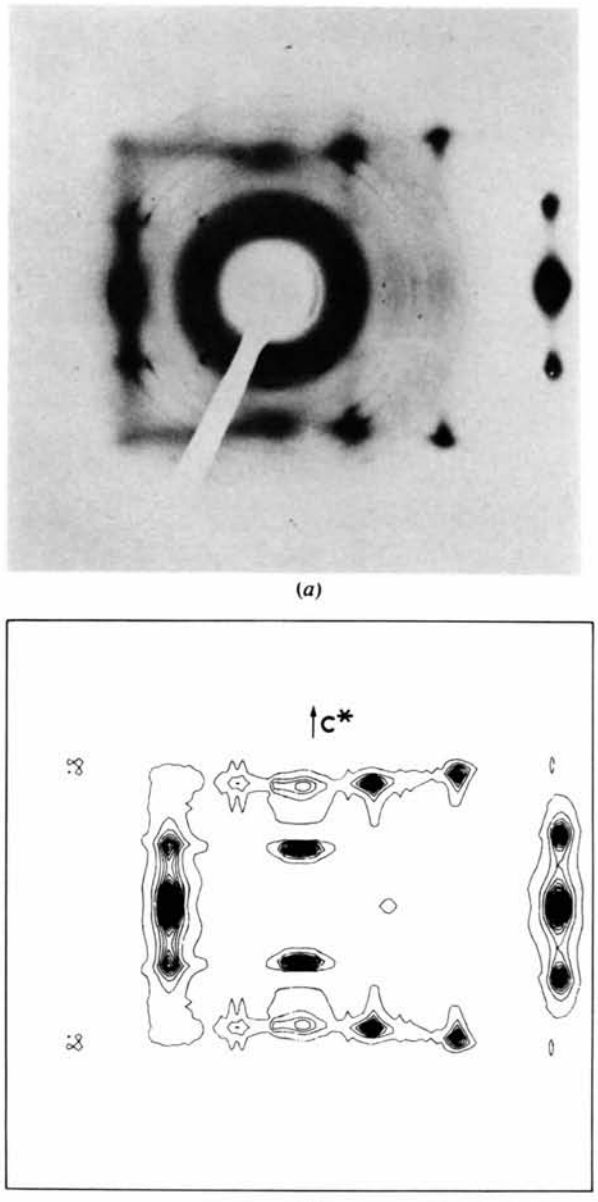

Fig. 9. Details as in Fig. 5; $\mathbf{c}^*$ parallel to the film, $\mathbf{a}_1^*$ inclined by 20° to the film.

Their **q** vector is parallel to **c*** and their amplitudes are perpendicular to **c***, showing that the ions move in shallow potentials. In these directions the Li(2) ions move easily with an activation energy of only 0·29 eV. The disc-like diffuse intensity is due to low-energy vibrations with a polarization vector parallel to **c***. The transversal B_2 branches of Fig. 3(*a*) have polarization vectors parallel to **c***. These vibrations can be considered as precursors of the Li(2)–Li(2) jumps parallel to **c** between Li_2N layers. This shows that there exists a close relationship between the main features of the diffuse scattering and the diffusion path of the Li(2) ions.

Comparison of the dispersion curves of Li_3N with those of other ionic crystals, *e.g.* alkali halides, shows that in both cases the lowest acoustic modes are found in the same frequency range whereas in superionic conductors like α-AgI very-low-frequency phonons are found. Therefore, it seems to be evident that the high ionic conductivity of Li_3N is at least partly due to intrinsic effects together with important contributions by defects and impurities.

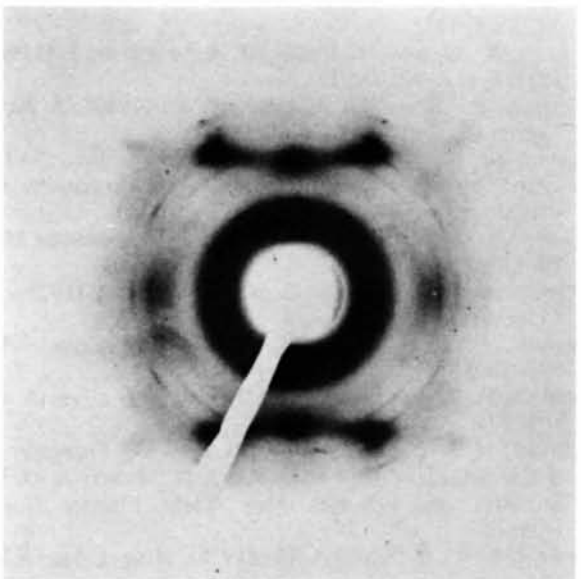

(*a*)

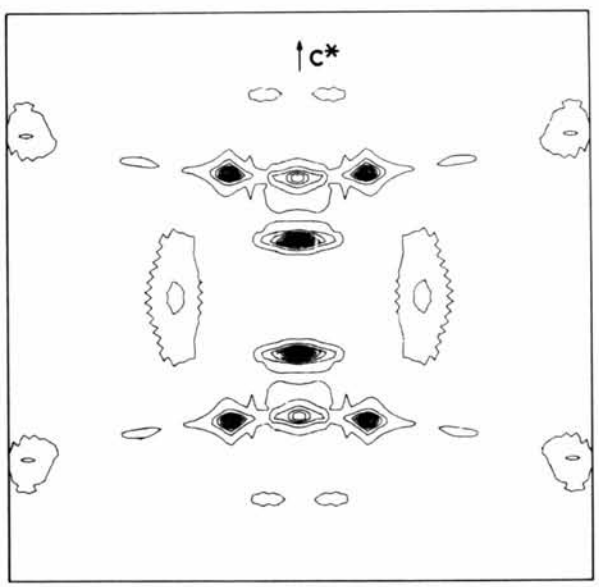

(*b*)

Fig. 10. Details as in Fig. 5; **c*** parallel to the film, $\mathbf{a}_1^*$ inclined by 30° to the film.

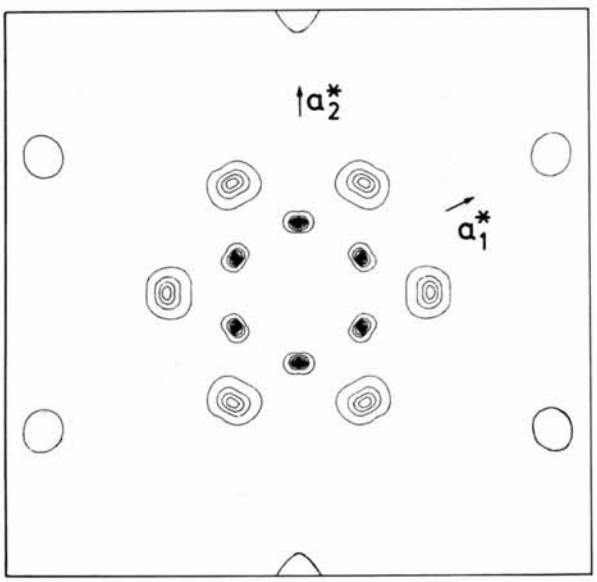

(*a*)

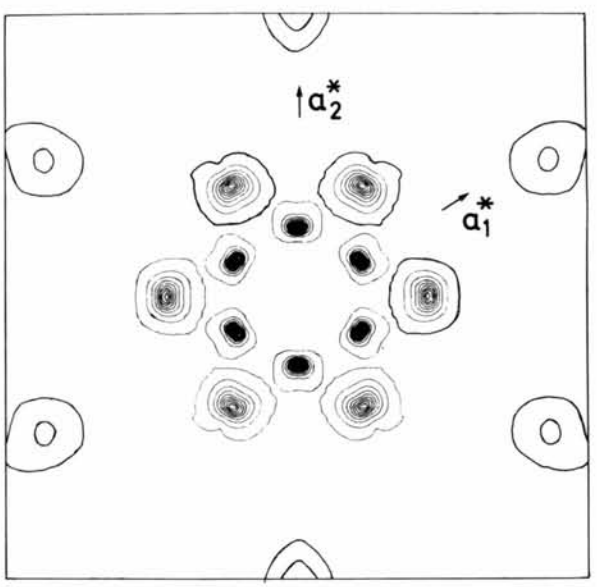

(*b*)

Fig. 11. Calculated intensity distribution for (*a*) 293 K, and (*b*) 673 K; ($\mathbf{a}_1^*$, $\mathbf{a}_2^*$) plane parallel to the film as in Fig. 5.

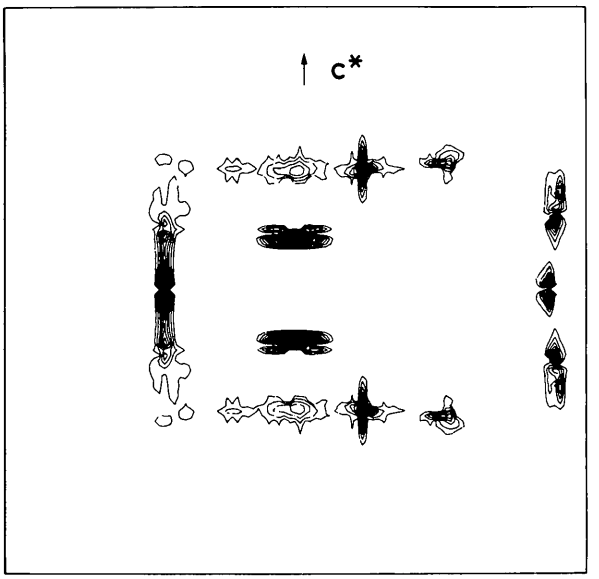

Fig. 12. Intensity distribution calculated with the lowest phonon modes only. Orientation as in Fig. 9.

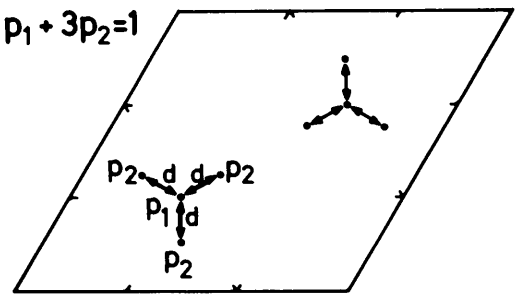

Fig. 13. Split model for Li(2) position. p_1 and p_2 occupation probabilities of the regular Li(2) and of the Li(2) split positions. d: split distance.

References

ALPEN, U. VON (1979). *J. Solid State Chem.* **29**, 379–392.

ALPEN, U. VON, BELL, M. F. & GLADDEN, T. (1979). *Electronchem. Acta*, **24**, 741–744.

ALPEN, U. VON, RABENAU, A. & TALAT, G. H. (1977). *Appl. Phys. Lett.* **30**, 621–623.

BOUKAMP, B. A. & HUGGINS, R. A. (1976). *Phys. Lett. A*, **58**, 231–233.

BRINKMANN, D., FREUDENREICH, W. & ROSS, J. (1978). *Solid State Commun.* **28**, 233–237.

CHANDRASEKHAR, H. R., BHATTACHARYA, G., MIGONI, R. & BILZ, H. (1978). *Phys. Rev. B*, **17**, 884–893.

DIFFERT, K. & MESSER, R. (1980). *J. Phys. C.* **13**, 717–724.

HUGGINS, R. A. & RABENAU, A. (1978). *Mater. Res. Bull.* **13**, 1315–1325.

KRESS, W., GRIMM, H., PRESS, W. & LEFEBVRE, J. (1980). *Phys. Rev. B.* **22**, 4620.

MESSER, R., BIRLI, H. & DIFFERT, K. (1980). *J. Phys. (Paris)*, **41**, Coll. 6, 28–31.

RABENAU, A. (1978). *Festkörperprobleme*, Vol. XVIII, edited by J. TREUSCH, pp. 77–108. Braunschweig: Pergamon/Vieweg.

RABENAU, A. & SCHULZ, H. (1976). *J. Less-Common Met.* **50**, 155–159.

SCHÖNHERR, E., MÜLLER, G. & WINKLER, E. (1978). *J. Cryst. Growth*, **43**, 467–472.

SCHULZ, H. & SCHWARZ, K. (1978). *Acta Cryst.* A**34**, 999–1005.

SCHULZ, H. & THIEMANN, K. H. (1979). *Acta Cryst.* A **35**, 309–314.

SCHULZ, H. & ZUCKER, U. (1979). *Fast Ion Transport in Solids*, edited by P. VASHISHTA, J. N. MUNDY & G. K. SHENOY, pp. 495–498. New York: Elsevier North Holland.

SCHWARZ, K. & SCHULZ, H. (1978). *Acta Cryst.* A**34**, 994–999.

WAHL, I. & HOLLAND, U. (1978). *Solid State Commun.* **26**, 229–233.

WILLIS, B. T. M. & PRYOR, A. W. (1975). *Thermal Vibrations in Crystallography*. Cambridge Univ. Press.

ZINTL, E. & BRAUER, G. (1935). *Z. Elektrochem.* **41**, 102–107.